Broadband stimulated Raman scattering spectroscopy by a photonic time stretcher

Francesco Saltarelli,[1,2] Vikas Kumar,[1] Daniele Viola,[1] Francesco Crisafi,[1] Fabrizio Preda,[1] Giulio Cerullo[1] and Dario Polli[1,*]

[1]*CNR-IFN and Dipartimento di Fisica, Politecnico di Milano, Piazza L. da Vinci 32, 20133 Milano (Italy)*
[2]*Universitá di Roma "La Sapienza", Dipartimento di Fisica, Roma, I-00185, Italy*
[*]*dario.polli@polimi.it*

Abstract: Stimulated Raman scattering spectroscopy is a powerful technique for label-free molecular identification, but its broadband implementation is technically challenging. We introduce and experimentally demonstrate a novel approach based on photonic time stretch. The broadband femtosecond Stokes pulse, after interacting with the sample, is stretched by a telecom fiber to ≈15ns, mapping its spectrum in time. The signal is sampled through a fast analog-to-digital converter, providing single-shot spectra at 80-kHz rate. We demonstrate ≈10^{-5} sensitivity over ≈500cm^{-1} in the C-H region. Our results pave the way to high-speed broadband vibrational imaging for materials science and biophotonics.

OCIS codes: (290.5910) Scattering, stimulated Raman; (300.6450) Spectroscopy, Raman; (320.7150) Ultrafast spectroscopy; (060.2310) Fiber optics.

References and links

1. M. Ghomi, *Applications of Raman spectroscopy to biology: from basic studies to disease diagnosis* (IOS, 2012).
2. W. H. Weber, R. Merlin, *Raman scattering in materials science* (Springer, 2000).
3. D. Pestov, R. K. Murawski, G. O. Ariunbold, X. Wang, M. C. Zhi, A. V. Sokolov, V. A. Sautenkov, Y. V. Rostovtsev, A. Dogariu, Y. Huang, and M. O. Scully, "Optimizing the laser-pulse configuration for coherent Raman spectroscopy," Science **316**(5822), 265–268 (2007).
4. G. Turrell and J. Corset, *Raman microscopy: developments and applications* (Academic, 1996).
5. W. Min, Ch. W. Freudiger, S. Lu, X.S. Xie, "Coherent nonlinear optical imaging: beyond fluorescence microscopy," Annu Rev Phys Chem **62**, 507–530 (2011).
6. A. Zumbusch, G. R. Holtom, and X. S. Xie, "Three-dimensional vibrational imaging by coherent anti-Stokes Raman scattering," Phys. Rev. Lett. **82**(20), 4142–4145 (1999).
7. C. L. Evans, E. O. Potma, M. Puoris'haag, D. Côté, C. P. Lin, and X. Sunney Xie, "Chemical imaging of tissue in vivo with video-rate coherent anti-Stokes Raman scattering microscopy," Proc. Natl. Acad. Sci. USA **102**(46), 16807–16812 (2005).
8. C. W. Freudiger, W. Min, B. G. Saar, S. Lu, G. R. Holtom, C. He, J. C. Tsai, J. X. Kang, and X. S. Xie, "Label-free biomedical imaging with high sensitivity by stimulated Raman scattering microscopy," Science **322**(5909), 1857–1861 (2008).
9. P. Nandakumar, A. Kovalev, and A. Volkmer, "Vibrational imaging based on stimulated Raman scattering microscopy," New J. Phys. **11**(3), 033026 (2009).
10. B. G. Saar, C. W. Freudiger, J. Reichman, C. M. Stanley, G. R. Holtom, and X. S. Xie, "Video-rate molecular imaging in vivo with stimulated Raman scattering," Science **330(**6009), 1368–1370 (2010).
11. M. T. Cicerone, K. A. Aamer, Y. J. Lee, and E. Vartiainen, "Maximum entropy and time-domain Kramers-Kronig phase retrieval approaches are functionally equivalent for CARS microspectroscopy," J. Raman Spectrosc. **43**(5), 637–643 (2012).
12. C. H. Camp Jr. and M. T. Cicerone, "Chemically sensitive bioimaging with coherent Raman scattering," Nat. Photon. **9**, 295–305 (2015).

13. C. H. Camp, Jr., Y. J. Lee, J. M. Heddleston, C. M. Hartshorn, A. R. H. Walker, J. N. Rich, J. D. Lathia, and M. T. Cicerone, "High-speed coherent Raman fingerprint imaging of biological tissues," Nat. Photonics **8**, 627–634 (2014).
14. R. Arora, G. I. Petrov, J. Liu, and V. V. Yakovlev, "Improving sensitivity in nonlinear Raman microspectroscopy imaging and sensing," J. Biomed. Opt. **16**(2), 021114 (2011).
15. T. W. Kee and M. T. Cicerone, "Simple approach to one-laser, broadband coherent anti-Stokes Raman scattering microscopy," Opt. Lett. **29**(23), 2701–2703 (2004).
16. H. Kano and H. Hamaguchi, "Femtosecond coherent anti-Stokes Raman scattering spectroscopy using supercontinuum generated from a photonic crystal fiber," Appl. Phys. Lett. **85**, 4298–4300 (2004).
17. B. von Vacano, L. Meyer, and M. Motzkus, "Rapid polymer blend imaging with quantitative broadband multiplex CARS microscopy," J. Raman Spectrosc. **38**, 916–926 (2007).
18. C. Pohling, T. Buckup, A. Pagenstecher, and M. Motzkus, "Chemoselective imaging of mouse brain tissue via multiplex CARS microscopy," Biomed. Opt. Express **2**(8), 2110–2116 (2011).
19. T. Hellerer, A. M. K. Enejder, and A. Zumbusch, "Spectral focusing: high spectral resolution spectroscopy with broad-bandwidth laser pulses," Appl. Phys. Lett. **85**, 25–27 (2004).
20. I. Rocha-Mendoza, W. Langbein, and P. Borri, "Coherent anti-Stokes Raman microspectroscopy using spectral focusing with glass dispersion," Appl. Phys. Lett. **93**, 201103 (2008).
21. J. P. Ogilvie, E. Beaurepaire, A. Alexandrou, and M. Joffre, "Fourier-transform coherent anti-Stokes Raman scattering microscopy," Opt. Lett. **31**(4), 480–482 (2006).
22. T. Ideguchi, S. Holzner, B. Bernhardt, G. Guelachvili, N. Picqué, and T. W. Hänsch, "Coherent Raman spectro-imaging with laser frequency combs," Nature **502**, 355–358 (2013).
23. K. Hashimoto, M. Takahashi, T. Ideguchi, and K. Goda, "Broadband coherent Raman spectroscopy running at 24,000 spectra per second," Sci. Rep. **6**, 21036 (2016).
24. E. Ploetz, S. Laimgruber, S. Berner, W. Zinth, and P. Gilch, "Femtosecond stimulated Raman microscopy," Appl. Phys. B **87**(3), 389–393 (2007).
25. E. Ploetz, B. Marx, T. Klein, R. Huber, and P. Gilch, "A 75 MHz light source for femtosecond stimulated Raman microscopy," Opt. Express **17**(21), 18612–18620 (2009).
26. W. Rock, M. Bonn, and S. H. Parekh, "Near shot-noise limited hyperspectral stimulated Raman scattering spectroscopy using low energy lasers and a fast CMOS array," Opt. Express **21**(13), 15113–15120 (2013).
27. Y. Ozeki, W. Umemura, Y. Otsuka, S. Satoh, H. Hashimoto, K. Sumimura, N. Nishizawa, K. Fukui, and K. Itoh, "High-speed molecular spectral imaging of tissue with stimulated Raman scattering," Nat. Photonics **6**, 845–851 (2012).
28. L. Kong, M. Ji, G. R. Holtom, D. Fu, C. W. Freudiger, and X. S. Xie, "Multicolor stimulated Raman scattering microscopy with a rapidly tunable optical parametric oscillator," Opt. Lett. **38**, 145–147 (2013).
29. S. Karpf, M. Eibl, W. Wieser, T. Klein, and R. Huber, "A time-encoded technique for fibre-based hyperspectral broadband stimulated Raman microscopy," Nat. Commun. **6**, 6784 (2015).
30. D. Fu, F.-K. Lu, X. Zhang, Ch. Freudiger, D.R. Pernik,G. Holtom, and X.S. Xie, "Quantitative chemical imaging with multiplex stimulated Raman scattering microscopy," J. Am. Chem. Soc. **134**, 3623–3226 (2012).
31. E. R. Andresen, P. Berto, and H. Rigneault, "Stimulated Raman scattering microscopy by spectral focusing and fiber-generated soliton as Stokes pulse," Opt. Lett. **36**(13), 2387–2389 (2011).
32. D. Fu, G. Holtom, C. Freudiger, X. Zhang, and X. S. Xie, "Hyperspectral imaging with stimulated Raman scattering by chirped femtosecond lasers," J. Phys. Chem. B **117**(16), 4634–4640 (2013).
33. K. Seto, Y. Okuda, E. Tokunaga, and T. Kobayashi, "Development of a multiplex stimulated Raman microscope for spectral imaging through multi-channel lock-in detection," Rev. Sci. Instrum. **84**(8), 083705 (2013).
34. K. Seto, Y. Okuda, E. Tokunaga, and T. Kobayashi, "Multiplex stimulated Raman imaging with white probe light from a photonic-crystal fibre and with multi-wavelength balanced detection," J. Phys. D **47**(34), 345401 (2014).
35. C.-S. Liao, M. N. Slipchenko, P. Wang, J. Li, S.-Y. Lee, R. A. Oglesbee, and J.-X. Cheng, "Microsecond scale vibrational spectroscopic imaging by multiplex stimulated Raman scattering microscopy," Light Sci. Appl. **4**, e265 (2015).
36. J. Réhault, F. Crisafi, V. Kumar, G. Ciardi, M. Marangoni, G. Cerullo, and D. Polli, "Broadband stimulated Raman scattering with Fourier-transform detection," Opt. Express **23**(19), 25235–25246 (2015).
37. A. Bhushan, F. Coppinger, and B. Jalali, "Time-stretched analogue-to-digital conversion," Electron. Lett. **34**(9), 839–841 (1998).
38. F. Coppinger, A. S. Bhushan, and B. Jalali, "Photonic time stretch and its application to analog-to-digital conversion," IEEE T. Microw. Theory **47**(7), 1309–1314 (1999).
39. A.M. Fard, S. Gupta, and B. Jalali, "Photonic time-stretch digitizer and its extension to real-time spectroscopy and imaging," Laser Photonics Rev. **7**(2), 207–263 (2013).
40. D. Solli, C. Ropers, P. Koonath, and B. Jalali, "Optical rogue waves," Nature **450**, 1054–1057 (2007).
41. G. Herink, B. Jalali, C. Ropers, and D. R. Solli, "Resolving the build-up of femtosecond mode-locking with single-shot spectroscopy at 90 MHz frame rate," Nat. Photonics **10**, 321–326 (2016).

42. M. Bradler, P. Baum, and E. Riedle, "Femtosecond continuum generation in bulk laser host materials with sub-μJ pump pulses," Appl. Phys. B **97**(3), 561–574 (2009).
43. D. Träutlein, M. Deibler, A. Leitenstorfer, and E. Ferrando-May, "Specific local induction of DNA strand breaks by infrared multi-photon absorption," Nucleic Acids Res. **38**(3), e14 (2010).
44. A. A. Voronin and A. M. Zheltikov, "Ionization penalty in nonlinear optical bioimaging," Phys. Rev. E **81**, 051918 (2010).
45. G. Agrawal, *Nonlinear fiber optics* (Academic, 2012).
46. M. Andreana, M.-A. Houle, D. J. Moffatt, A. Ridsdale, E. Buettner, F. Légaré, and A. Stolow, "Amplitude and polarization modulated hyperspectral stimulated Raman scattering microscopy," Opt. Expr. **23**(22), 28119–28131 (2015).
47. P. Berto, E. R. Andresen, and H. Rigneault, "Background-free stimulated Raman spectroscopy and microscopy," Phys. Rev. Lett. **112**, 053905 (2014).
48. C. H. Camp Jr., S. Yegnanarayanan, A. A. Eftekhar, H. Sridhar, and A. Adibi, "Multiplex coherent anti-Stokes Raman scattering (MCARS) for chemically sensitive, label-free flow cytometry," Opt. Expr. **17**(25) 22879-22889 (2009).
49. G. V. Oshovsky, G. Rago, J. P. R. Day, M. L. Soudijn, W. Rock, S. H. Parekh, G. Ciancaleoni, J. N. H. Reek, and M. Bonn, "Coherent anti-Stokes Raman scattering microspectroscopic kinetic study of fast hydrogen bond formation in microfluidic devices," Anal. Chem. **85**(19), 8923–8927 (2013).
50. M. Windbergs, M. Jurna, H. L. Offerhaus, J. L. Herek, P. Kleinebudde, and C. J. Strachan "Chemical imaging of oral solid dosage forms and changes upon dissolution using coherent anti-Stokes Raman scattering microscopy," Anal. Chem. **81**(6), 2085–2091 (2009).
51. F. Preda, V. Kumar, F. Crisafi, D. G. Figueroa Del Valle, G. Cerullo, and D. Polli, "Broadband pump-probe spectroscopy at 20-MHz modulation frequency," Opt. Lett. **41**(13), doc. ID 263685 (Posted 25 May 2016, in press).
52. P. R. Poulin and K. A. Nelson, "Irreversible organic crystalline chemistry monitored in real time," Science **313**(5794), 1756–1760 (2006).

1. Introduction

Raman spectroscopy is a powerful technique for label-free identification of molecules, based on their characteristic vibrational fingerprint. It finds applications in biomedical optics, for imaging and quantitative analysis of cells and tissues [1], in materials science [2] and in the standoff detection of airborne species [3]. The simplest Raman spectroscopy technique is spontaneous Raman [4], in which a quasi-monochromatic laser excites the molecule to a virtual state, which then relaxes to the ground state emitting photons at lower, Stokes-shifted frequencies. Spontaneous Raman measures the full vibrational spectrum, providing a detailed picture of the biochemical composition of the substances being measured [1]. However, due to the intrinsically low Raman cross section, it only gives very weak signals, resulting in low acquisition speeds, of the order of seconds per spectrum.

This speed limitation can be overcome by Coherent Raman Scattering (CRS) [5], a class of third-order nonlinear optical techniques that drive the sample with a pair of light pulses –the so-called pump (at frequency ω_p) and Stokes (at frequency ω_S). When the difference between pump and Stokes frequencies matches a vibrational frequency Ω, i.e. $\omega_p - \omega_S = \Omega$, then the molecules in the focal volume are resonantly excited and vibrate in phase; this vibrational coherence enhances the Raman response by many orders of magnitude with respect to the incoherent spontaneous Raman process.

The two most widely employed CRS techniques are Coherent Antistokes Raman Scattering (CARS) [6,7] and Stimulated Raman Scattering (SRS) [8-10]. In the CARS process the vibrational coherence is read by a further interaction with the pump beam, generating a coherent radiation at the anti-Stokes frequency $\omega_{aS} = \omega_p + \Omega$. In SRS the coherent interaction with the sample induces stimulated emission from a virtual state of the sample to the investigated vibrational state, resulting in a Stokes-field amplification (called Stimulated Raman Gain, SRG) and in a simultaneous pump-field attenuation (called Stimulated Raman Loss, SRL). CARS is free from linear background as it detects a signal at ω_{aS} that is blue-shifted with respect to the pump and Stokes pulses. On the other hand, CARS is affected by a non-resonant background (NRB), due to four-wave-mixing, which prevents a straightforward extraction of quantitative information, unless using complex phase-retrieval algorithms [11] that can hardly be

implemented at high speeds. Furthermore, the CARS response scales quadratically with the number of oscillators in the focal volume, making it very hard to quantify concentrations and to probe dilute species. These drawbacks of CARS are overcome by SRS, which does not suffer from NRB and inherently provides a linear dependence of the signal on the concentration of the sample. The technical challenge of SRS lies in the requirement to detect a weak differential signal (SRG or SRL) on top of a large linear background (the Stokes or the pump pulse). This is typically accomplished by high-frequency (a few MHz) amplitude modulation of one of the laser beams (pump or Stokes) followed by lock-in detection of its counterpart (Stokes or pump), which enables one to reach shot noise limited sensitivity.

Current implementations of CRS, while achieving extremely high acquisition speeds up to the video rate [7,10], mostly work at a single frequency, with narrowband pump and Stokes pulses, thus providing limited chemical information. The extension of CRS to the broadband regime is technically challenging [12]. Broadband CARS [13,14] can be implemented by replacing (i) the narrowband pump or Stokes pulse with a broadband pulse generated in a tapered optical fiber [15] or a photonic crystal fiber [16, 17] and (ii) the single-pixel detector (typically an avalanche photodiode or a photomultiplier) with a (cooled) CCD or a photodiode array with hundreds or thousands of pixels. In this way, a very large spectral coverage [18] can be reached, ultimately over the entire Raman band. The pixel dwell time in this case is often limited to a few milliseconds by the read-out speed of the camera. Cicerone and coworkers, taking advantage of the heterodyne amplification of weak CARS signals via the NRB and employing phase retrieval methods [11], demonstrated background-free Raman microscopy with linear dependence on the sample concentration down to the fingerprint region [13]. Hyperspectral CARS imaging has also been demonstrated by sequentially recording single-colour CARS signals at different frequencies by simply varying the delay between broadband femtosecond pump and Stokes pulses chirped up to a few picoseconds using a spectral focusing technique [19,20]. Finally, broadband CARS has been demonstrated using a Fourier transform approach, in which the CARS signal is detected in the time domain as the modulation induced by the vibrational coherence on a time-delayed probe pulse [21-23].

First attempts to realize broadband SRS were based on slow (readout rates up to a few kHz) optical multichannel analyzers (OMAs) [24-25], resulting in a very long measurement time, also due to the intrinsic shot noise of the detectors (limited by the 10^4–10^6-electrons full-well capacity of each pixel, corresponding to 10^{-2}–10^{-3} maximum SRS sensitivity for a single couple of pump-on/pump-off spectra [26]). Hyperspectral SRS was achieved using the so-called swept-source approach, in which narrowband picosecond pulses are rapidly tuned using either a wavelength scanner [27] or an optical parametric oscillator equipped with an electro-optical filter [28]. Recently, Huber and coworkers demonstrated a low-cost fiber-based version of the swept-source SRS technique, based on a rapidly tunable continuous-wave laser, providing excellent spectral resolution (< 3 cm^{-1}) and very large spectral coverage [29]. Another method uses an acousto-optical tunable filter to modulate the various spectral portions of a broadband pulse at different frequencies, so that the SRS spectrum can be reconstructed by demodulating the signal at different frequencies [30]. As with CARS, spectral focusing based on chirped femtosecond pulses can also be applied to multiplex SRS [31,32] and provides quantitative Raman images free from NRB at high speed. Parallel detection of broadband SRS spectra has been performed with a multi-channel lock-in amplifier but only at low modulation frequencies (a few kHz), again limiting the sensitivity [33,34]. Much better results were obtained using a multi-channel active filter, in which a series of special electronic band-pass filters and trans-impedance amplifiers were tuned to specifically extract and amplify only the signal at the modulation frequency of the pump pulse [35]. Finally, a proof of principle of time-domain Fourier-transform detection of the broadband SRS spectrum was recently performed using a passive birefringent interferometer [36].

Photonic time stretch (PTS) spectroscopy, also known as dispersive Fourier transform, is a powerful technique for single-channel measurement of optical spectra at high repetition rates

[37-39]. It consists in temporally stretching the pulse to be measured, typically by a long optical fiber, to a duration of a few nanoseconds, so that it can be accurately sampled by a high-frequency analog to digital converter (ADC). By calibrating the dispersion introduced by the optical fiber, each point of the sampled temporal profile can be uniquely associated with a wavelength, allowing measurement of spectra at repetition rates up to tens of MHz. PTS, with its unique capability to measure single-shot spectra at high repetition rates, has found application in the detection of optical rogue waves [40] and in the study of dynamical processes, such as the onset of the mode-locking regime [41].

In this paper, we apply the PTS approach to the detection of broadband SRS spectra. The concept of PTS-SRS is quite simple: a narrowband pump and a broadband Stokes pulse are combined, the pump is modulated and the Stokes spectra after the sample are detected by the PTS technique at high speed. Using a laser system running at 80-kHz repetition rate, we demonstrate the acquisition of broadband SRS spectra across the CH stretching band (2700-3250 cm^{-1}) with sensitivity well below 10^{-4}. By a proper optimization of the excitation source, we anticipate a significant increase of the detection bandwidth and the acquisition speed.

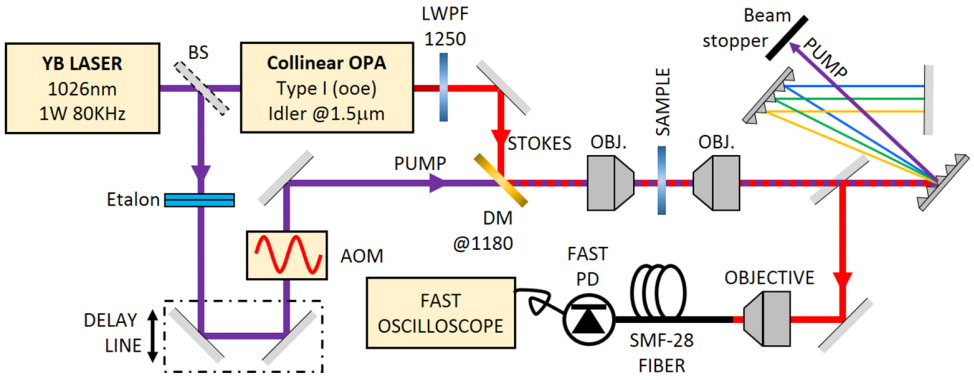

Fig. 1. Experimental setup of the PTS-SRS. BS: beam splitter; AOM: Acousto-optic modulator; LWPF: long-wave-pass filter; DM: dichroic mirror; OBJ., microscope objectives; PD: photodiode.

2. Experimental setup

Our PTS-SRS system is depicted in Fig. 1. It starts with a regeneratively amplified Yb:KGW laser (Pharos, Light Conversion) generating 290-fs pulses at 1026 nm with 80-kHz repetition rate. For our experiments we used an average power of 1 W, corresponding to 12.5-µJ pulse energy. The laser output is divided in two arms: the first one generates the narrowband pump pulses and the second one the broadband Stokes pulses. The pump pulses are directly obtained from the laser output by spectral filtering with an etalon (SLS Optics Ltd.), with 14% throughput, resulting in 1026-nm pump pulses with 8-cm^{-1} bandwidth and >350 nJ pulse energy. The pump pulse duration is ≈1,7ps, as measured by autocorrelation. The remaining 10-µJ fraction of the output drives a collinear optical parametric amplifier (OPA), pumped by the second harmonic at 513 nm and seeded by a white light continuum (WLC) generated in a 6-mm-thick YAG plate [42]. By amplifying the portion of the WLC around 785 nm, we obtain an idler with ≈50-nm FWHM bandwidth tunable in the 1420-1540 nm range, covering a frequency detuning of ≈400 cm^{-1} in the 2700-3250 cm^{-1} region, enabling full coverage of the CH-stretching band. Typical pulse energy of the idler is ≈80nJ, which is more than sufficient for our experiments (utilizing only ≈1nJ Stokes pulse energy on the sample). The chosen Stokes wavelength enables straightforward temporal stretching in a standard SMF-28 telecom fiber. Furthermore, the combination of pump and Stokes wavelengths at 1µm and 1.5µm, respectively, enables us to minimize photodamage [14,43,44] due to multi-photon absorption in DNA and proteins in the ≈260-nm region, which is a four-photon process for the pump and a five/six-

photon process for the Stokes. We note that the (linear) water absorption coefficient is quite high for the Stokes pulse (α=10-20 cm^{-1} between 1.4 and 1.55 μm) but for imaging single cells (with thickness of a few micrometers) or thin tissue slices (with a thickness reaching a few tens of micrometers) the overall absorption of the (weak) Stokes light would be limited to a few percent, which is negligible in most applications. On the other hand, the water absorption coefficient of the (intense) pump pulse at 1μm is much weaker (α=0.3 cm^{-1}).

The pump pulse is modulated at 20-kHz frequency by an acousto-optic modulator. We could not modulate it at half the repetition rate of the laser because we observed a residual intensity modulation at 40 kHz that spoiled the measurement quality, probably due to a resonance in the Pockels cell of the Yb laser. Pump and Stokes, synchronized by a delay line, are collinearly combined by a dichroic beam splitter and focused on the sample by a 20×, NA=0.3 microscope objective with >90% transmission for both the pump and the Stokes wavelengths. After the sample, the transmitted Stokes, recollimated by a second objective, is sent to the PTS and the detection chain. To avoid nonlinear pulse distortions in the fiber, the pulse is pre-stretched using a grating pair (ruled reflective diffraction gratings with 600 grooves/mm and different size, models GR50-0616 and GR13-0616 from Thorlabs), placed at ~28-cm distance. This introduces negative dispersion (GDD ≅ - 1.2 ps^2) to the pulse, bringing it from 130 fs to ~33 ps (as measured by autocorrelation) and lowering its peak power enough to allow neglecting non-linearities in the fiber. The majority of the stretching is performed using a single-mode telecom fiber (Corning SMF28), providing a negative dispersion of $D = 11.3\, ps/\left(nm \cdot km\right)$ around λ=1460nm. We have employed a fiber with L=18.65 km length, stretching the Stokes pulse to a ~15-ns duration. The fiber displays very low losses in this wavelength range, in the 0.2-0.4 dB/km (depending on the wavelength), resulting in a total attenuation <7 dB. The overall throughputs of the grating stretcher and the fiber stretcher (also considering the insertion losses, and the losses of the fiber connectors and the objectives) are ~15% and ~12%, respectively, which still yields enough pulse energy to allow detection by a fast photodiode (Teledyne LeCroy model OE 455, 3.5 GHz bandwidth, 1 V/mW responsivity) and analog to digital conversion through a high-bandwidth digital oscilloscope. We note that we could easily improve the throughput of the grating stretcher by at least a factor of four, if needed, employing a higher-quality grating pair. We could also replace the grating stretcher by a silicon prism pair, that would not only provide almost unitary throughput but it would also make the experimental setup more compact and easier to align. We compared two oscilloscope models: the first one (Teledyne LeCroy Waverunner 8254M) with higher bandwidth (2.5 GHz, 40 GS/s sampling rate) but lower resolution (8-bit digitization) and the second (Teledyne LeCroy HDO6104) with lower bandwidth (1 GHz, 2.5 GS/s sampling rate) but higher resolution (12-bit digitization).

3. Results and discussion

We first performed a calibration of the PTS spectrometer. Figure 2(a) shows as a red solid line the temporal trace of the Stokes pulse recorded by the 12-bit 1-GHz oscilloscope, obtained by averaging 100 consecutive time traces. It lasts in total ~15ns, corresponding to ~40 samples. We note that it is not possible to trigger the oscilloscope using a reference signal from the laser itself, because such a trigger signal has a jitter of 1-2ns, which is much larger than the required precision. Furthermore, the total propagation time of a Stokes pulse through the fiber is ≈90 μs, more than 7 times longer than the pulse repetition period, so that external triggering from the laser sync signal would prevent acquisition of all laser shots. For these reasons, we designed a cross-correlation algorithm to post-process the acquired data and temporally align the traces. This results in ≈2-fold better performances with respect to a simple "level" trigger on the Stokes trace itself.

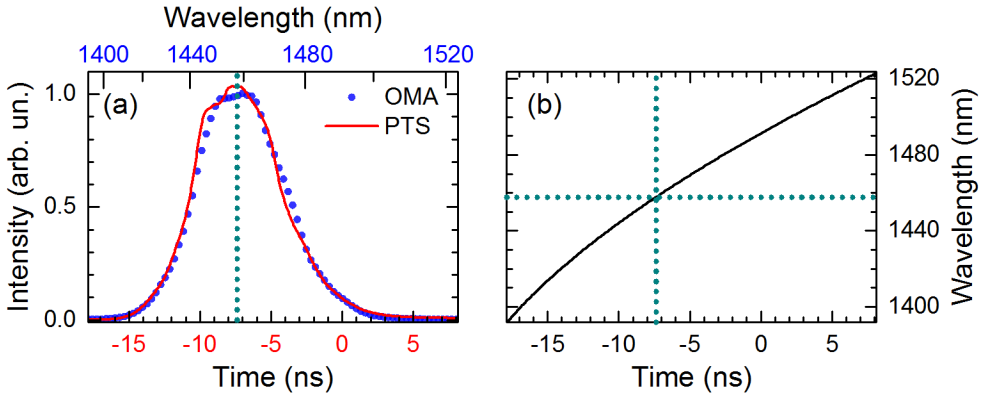

Fig. 2. Calibration of the PTS. (a) Stokes temporal traces acquired with the oscilloscope (red continuous line) and corresponding Stokes spectrum acquired with the OMA (blue dotted line) (b) Time-wavelength calibration curve.

Figure 2(a) also shows the corresponding Stokes spectrum measured by a conventional OMA as a blue dotted line. We can see that there is a very good agreement between the two techniques. The small deviations of the two curves are due to the different, wavelength-dependent coupling of the light through the OMA aperture slit with respect to the optical fiber. They do not constitute a problem, however, since the SRS spectra are differential signals (i.e. they always require normalization of the Stokes spectral change induced by the pump with respect to the Stokes spectrum itself).

The matching between the temporal trace acquired by the fast photodiode and the spectrum measured by the OMA is guaranteed via a time-spectrum calibration procedure. The dispersion introduced by the grating pair can be neglected with respect to that introduced by the fiber, so that we consider only the latter for the calibration of the PTS-SRS. By integrating the well-characterized dispersion curve D(λ) of our Corning SMF-28 telecom fiber over the wavelength, considering the total length L of the fiber, we easily obtain [45] the relative arrival time of the various wavelengths of the Stokes pulse at the photodiode:

$$T(\lambda) = T(\lambda_0) + \int_{\lambda_0}^{\lambda} D(\lambda') \cdot L \cdot d\lambda'$$

The calibration thus only requires one input information, which is the arrival time $T(\lambda_0)$ of a specific wavelength λ_0. As the dispersion curve D(λ) is non-linear, one cannot overlap the two signals from the OMA and the PTS. To overcome this problem, we considered a sufficiently narrow portion of the two signals (from the OMA and the PTS) around the peak (so that the dispersion is approximately linear) and matched their centroid [vertical dotted line in Fig. 2(a)]. The calibration curve obtained by this procedure is shown in Fig. 2(b). The horizontal and vertical dotted lines represent the single-point calibration λ_0 and T(λ_0). In this way, we can map the time axis of the oscilloscope into the wavelength axis of the Stokes pulse.

This calibration procedure also allows us to retrieve the spectral resolution of the PTS-SRS setup. For the region of interest (1420-1540 nm range, corresponding to approx. 2700-3250 cm^{-1} Raman shift) the calibration curve has a slope of ~5nm/ns, corresponding to C~25cm^{-1}/ns in terms of Raman shift. The 12-bit (8-bit) oscilloscope has a sampling rate of 2.5 GS/s (40 GS/s), so that we acquire a sample every ~10 cm^{-1} (~0.6 cm^{-1}), and a bandwidth of B=1GHz (2.5 GHz), limiting the spectral resolution to C/B~25cm^{-1} (~10cm^{-1}). Recalling that the pump pulse has 8 cm^{-1} spectral bandwidth, determined by the transmission spectrum of the etalon, we conclude that the bandwidth of the oscilloscope is the limiting factor in determining the final spectral resolution of the SRS experiment. To improve it, one would simply need to further increase the fiber length or to replace it with a more dispersive one; this would also lead to higher losses,

which would be tolerable because we are not employing the full energy of the Stokes and the pre-stretching grating pair guarantees negligible non-linearities in the fiber.

Figure 3(a) reports the calibrated Stokes spectra in the absence ($I_{OFF}(\lambda)$, red curve) and in the presence ($I_{ON}(\lambda)$, black curve) of the pump pulse, respectively, each averaged over 100 laser shots, for a methanol sample contained in a cuvette with 1-mm optical path. In this experiment and in the following, the Stokes power at the sample was kept below 80 μW, which is well below the sample damage threshold but still enough for reaching a sufficiently high voltage at the photodiode (almost 1V) considering the throughput of the collecting objective and of the grating/pulse stretchers. Figure 3(b) shows the resulting $SRG(\lambda) = \left[I_{ON}(\lambda) - I_{OFF}(\lambda) \right] / I_{OFF}(\lambda)$ spectrum as a black solid line. We can recognize the typical Raman peaks of methanol at 2840 and 2940 cm^{-1} (corresponding to the symmetric and antisymmetric CH_3 stretching mode, respectively). For comparison, we also reported as a dashed orange line the spontaneous Raman spectrum of methanol. Note that temporal alignment of the two pulses is crucial in order to perform an accurate subtraction; this is achieved by temporally shifting one of the two pulses until their cross-correlation is maximized. While this procedure is well suited for low SRG signals, it starts failing for high SRG because the $I_{OFF}(\lambda)$ and $I_{ON}(\lambda)$ spectral shapes differ significantly; in this case, we rely on a simple "level" trigger.

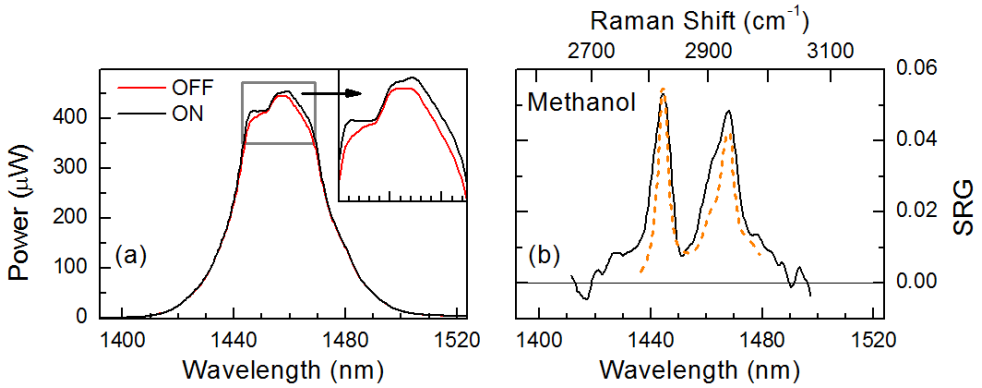

Fig. 3. (a) Stokes spectra obtained with the PTS setup in the presence (black line) and in the absence (red line) of the pump pulse. The inset highlights the spectral differences due to SRG in the methanol sample. (b) Corresponding SRG spectrum of methanol obtained by PTS-SRS technique (black solid line). As a dashed orange line we also reported a reference spontaneous Raman spectrum of methanol, adapted from [8].

The SRS signal displayed in Fig. 3(b) is rather intense, corresponding to a SRG of approximately 5%. Many applications, especially in biomedical optics, call for the detection of much weaker signals. To this end, we evaluated the achievable sensitivity with our PTS-SRS set-up for both oscilloscopes, performing a series of measurements with increasing number of spectra from N=4 (equivalent to two Stokes spectra with the pump and two without it) to N= 65,000 (for the 12-bit oscilloscope) and N=15,000 (for the 8-bit oscilloscope), corresponding in both cases to the maximum number of samples to fill the available memory. Figure 4(a) reports the sensitivity (i.e. the rms SRG signal in the absence of any sample or pump pulses) of the 12-bit oscilloscope, which provided the best results, as a function of the number N of acquired spectra and the wavelength (lower scale) or Raman shift (upper scale). The noise of the measured spectral difference [$I_{ON}(\lambda)$-$I_{OFF}(\lambda)$] is flat and the resulting concave shape is only due to the normalization with respect to the Stokes spectrum. Using a flat-top Stokes spectrum one could thus reach the same sensitivity across the entire spectral region of interest. Figure 4 demonstrates that we can reach 10^{-5} sensitivity, typically required for detecting SRG signals of dilute species in biological microscopy applications [35], in less than 1-second measurement time.

Figure 4(b) reports the sensitivity averaged over the 2850-3200 cm^{-1} region for varying number of laser shots N for the 12-bit (circles) and the 8-bit (triangles) oscilloscopes in a log-log scale. For both cases, the sensitivity follows the predicted $1/\sqrt{N}$ dependence for uncorrelated random noise (see gray dashed lines). This demonstrates that the shot-to-shot total fluctuations of the system (e.g. laser fluctuations, shot noise, detector noise) are larger than the quantization noise. The latter is formally equal to $1/2^8 \approx 4 \cdot 10^{-3}$ for the 8-bit oscilloscope and $1/2^{12} \approx 2.4 \cdot 10^{-4}$ for the 12-bit oscilloscope, but higher in practice due to non-idealities in the ADC such as noise, non-linearity, gain and offset errors and distortions introduced by the front end of the oscilloscope, thus reducing the effective number of bits (ENOB). We also note that, on average, the sensitivity is twice better for the 12-bit oscilloscope, which is therefore preferable for SRS microscopy applications where the SRG levels are typically very small.

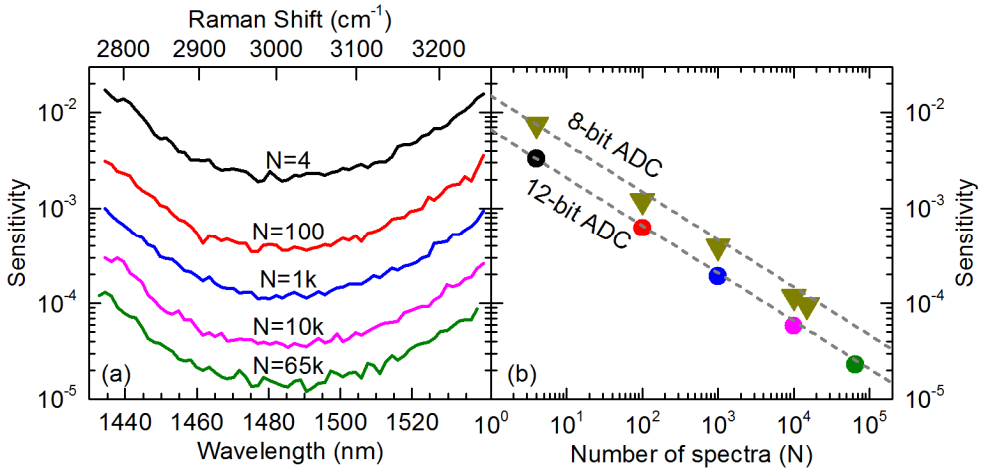

Fig. 4. Sensitivity of the PTS-SRS. (a) Wavelength-dependent rms of the SRG for different numbers of laser shots N, measured with the 12-bit oscilloscope. (b) rms of the SRG as a function of N for the 8-bit (triangles) and the 12-bit (circles) oscilloscopes. Dashed lines are fits to the data with $a/\sqrt{N}$ functions.

We applied our PTS-SRS instrument to the measurement of the Raman spectra of various solvents: methanol, cyclohexane, acetone and isopropanol. Figures 5(a) and 5(b) report the results for the 12-bit and the 8-bit oscilloscopes, respectively. While the 8-bit oscilloscope provides a better spectral resolution, the results are very similar and demonstrate the capability of the instrument to reveal the Raman peaks of different samples in the high-wavenumber region. We note that our spectral resolution is sufficient to distinguish, for example, not only the 2840 and 2940 cm^{-1} main peaks of methanol but also the shoulder at ≈2915 cm^{-1} with high accuracy [see also the comparison with the spontaneous Raman spectrum, orange dashed line in Fig. 5(b)]. Similarly, we do not only detect the major peak of acetone at 2920 cm^{-1} but also its red-shifted shoulder at ≈2960 cm^{-1}. In particular, the high-speed 8-bit oscilloscope is also capable of distinguishing the doublet of cyclohexane at ≈2925 and ≈2940 cm^{-1}. This confirms the high spectral resolution achievable with our PTS-SRS instrument. We note the presence of small modulations in the acetone spectrum in the 2800-2850 cm^{-1} spectral region: since they are consistently reproducible (compare the SRG spectra measured with the 8-bit and the 12-bit oscilloscope) but not present in the spontaneous Raman spectra, we attribute them to cross-phase modulation [46,47] between pump and Stokes pulses in the sample.

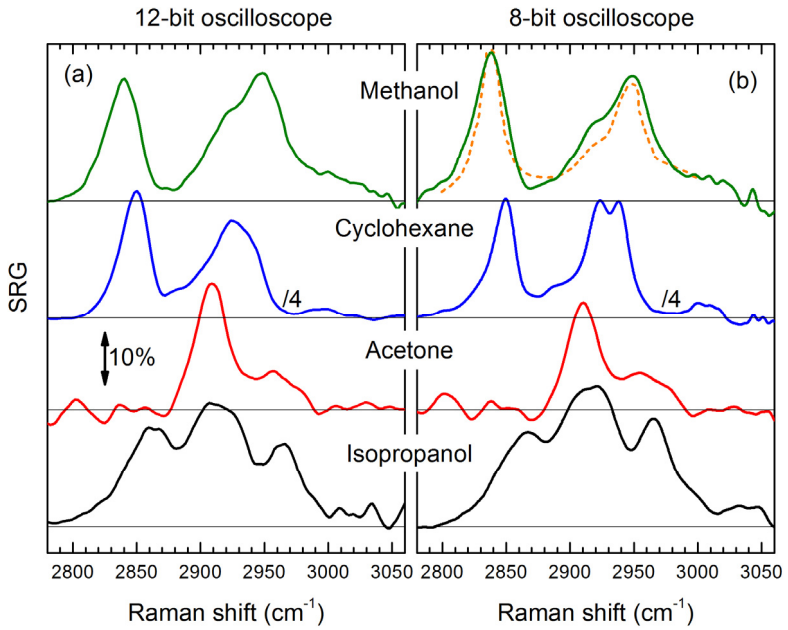

Fig. 5. SRS spectrum of different solvents. Each spectrum is obtained acquiring N=8 consecutive pulses (100µs acquisition time) for the 12-bit (a) and 8-bit (b) oscilloscope. Orange dashed line in (b) is a reference spontaneous Raman spectrum of methanol, adapted from [8]. Pump energy was 200nJ on the sample. The cyclohexane signal has been divided by 4 for comparison.

We measured the SRG spectrum of acetone using the PTS-SRS setup at various pump fluences, in order to confirm the achievable sensitivity and the linearity of the signal with the pump intensity. In Fig. 6(a) we plot the peak of the SRG signal at 2920 cm^{-1} (measured with the 12-bit oscilloscope) as a function of the pump energy in a log-log scale (brown circles), together with a linear fit. The inset reports an SRG spectrum measured in acetone at low pump energy (as indicated by the green arrow). Finally, we performed a dilution test of methanol in water, again with the 12-bit oscilloscope [Fig. 6(b)]. From top to bottom, starting from pure methanol, we halved its concentration at each consecutive run, down to ≈1.6%. The intensity of the SRG signal at 2840 cm^{-1} due to the methanol symmetric CH_3 stretching mode is plotted in the inset as a function of its concentration, together with a linear fit. This confirms the expected linear concentration dependence of SRS and demonstrates its capability to detect dilute species.

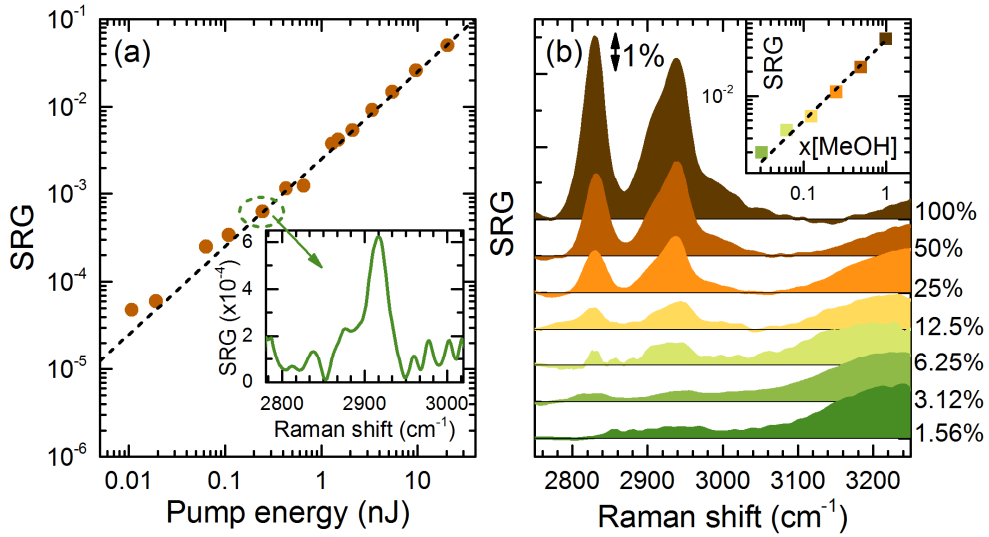

Fig. 6: (a) SRG on the acetone peak at 2940cm^{-1} as a function of the pump energy. Measurements were performed using the 12-bit oscilloscope. Inset: SRS spectrum of acetone acquired with 0.27-nJ pump energy and averaging over 10^4 laser shots (125-ms total measurement time). (b) Dilution test of methanol in water. Inset: SRG of the 2840 cm^{-1} peak as a function of methanol concentration.

4. Conclusions

In this paper we demonstrated a novel approach to broadband SRS, employing the photonic time stretch approach to detect single-shot spectra at high repetition rates. With our current implementation, using an 80-kHz repetition-rate laser, we covered a spectral window of 500 cm^{-1}, in the C-H stretching region, with frequency resolution of ≈10 cm^{-1} and a sensitivity of 10^{-3} in 400 µs and approaching $2 \cdot 10^{-5}$ for 1-second acquisition time. These performances are already suitable for a number of applications, such as monitoring microfluidic flows [48], the onset of chemical reactions [49] or solid-state samples such as pharmaceutical products [50].

We anticipate three major future developments of the instrument. First, tuning the OPA to the 1200-1300 nm wavelength region, we could extend the spectral coverage of SRS to the fingerprint region. One of the great advantages of the PTS-SRS technique, in fact, is that acquisition speed does not depend upon the covered spectral region. Second, using commercially available 5-MHz Yb amplified lasers with ≈10-µJ pulse energy (sufficient for both seeding the OPA stage and generating the pump pulses), we could shorten the acquisition time considerably, down to 6 µs for 10^{-3} sensitivity and 16 ms for $2 \cdot 10^{-5}$ sensitivity. This result paves the way to high-speed coherent Raman imaging of samples with their entire vibrational signature, which is the third goal we are planning to achieve. As recently excellently reviewed by Camp and Cicerone [12], the fastest acquisition time for the entire vibrational signature over both the fingerprint and the C-H stretching region ranges in the 1-10 ms per spectrum, using either broadband CARS [13] or spectral-focusing CARS [20]. With the aforementioned full Raman spectral coverage and acquisition speed, the PTS technique could be the first based on SRS to reach or eventually even overcome state-of-the-art competing experimental setups.

As a perspective, this technique could also be applied to pump-probe spectroscopy [51], which is a third-order nonlinear process very similar to SRS. The only differences are: (i) the pump pulse is tuned in resonance with an electronic absorption transition of the sample; (ii) the pump pulse can have a broader spectral bandwidth, corresponding to a pulse profile with sub-ps duration, so that the temporal resolution can be of the order of 100-fs or even better; (iii) the Stokes pulse is called probe; (iv) the temporal delay between the pump and probe pulses is not anymore fixed at zero but rather scanned from negative to positive delays, in order to follow

excited-state dynamics. On the one hand, a PTS-based pump-probe setup would allow one to achieve a broad spectral coverage with the high sensitivity typical of laser sources with MHz repetition rates, overcoming the problem of the absence in the market of line-scan cameras or CCDs with high dynamic range and μs-level refresh rate [51]. On the other hand, it would also allow one to track in real time irreversible photochemical reaction dynamics in the case of sample scarcity or product accumulation, that would otherwise require multiple laser shots [52]. The latter approach would require a relatively narrowband probe pulse with ≈100-fs transform-limited duration but stretched to several-picosecond duration on the sample, matching the overall temporal scale of the photoinduced dynamical processes to be studied, partially overlapped in time with the pump (with ≈100-fs duration) so that its major portion lies at positive time delays. After the sample, a PTS setup would allow one to stretch the probe pulse to the nanosecond temporal regime, so that the photo-induced sample dynamics, mapped in time onto the probe pulse temporal profile, would be measured with a fast digital-to-analogue converter.

Funding
European Research Council: Consolidator Grant VIBRA (ERC-2014-CoG No. 648615), Advanced Grant STRATUS (ERC-2011-AdG No. 291198) and Proof of Concept Grant MISSION (ERC-2014-POC No. 665635).

Acknowledgments
We acknowledge Dr. C. Manzoni, H. Hedayat, D. Bugini and E. Carpene for useful experimental help, Prof. P. Boffi for providing the optical fiber, G. Fabbro for lending the oscilloscopes.